34th Annual International Conference of the IEEE EMBS
San Diego, California USA, 28 August - 1 September, 2012

# High Acceleration with a Rotating Radiofrequency Coil Array (RRFCA) in Parallel Magnetic Resonance Imaging (MRI)

Mingyan Li[1], Jin Jin[1], Adnan Trakic[1], Feng Liu[1], Ewald Weber[1], Yu Li[1], Stuart Crozier[1], *Member, IEEE*

***Abstract*—This study explores the performance of a novel hybrid technology, in which the recently introduced rotating RF coil (RRFC) was combined with the principles of Parallel Imaging (PI) to improve the quality and speed of magnetic resonance (MR) images. To evaluate the system, a low-density naturally-decoupled 4-channel rotating radiofrequency coil array (RRFCA) was modelled and investigated. The traditional SENSitivity Encoding (SENSE) reconstruction method and the means of calculating the geometry factor distribution (g map) were adapted to take into account the transient sensitivity encoding. It was found from simulations at 3T that, continuous rotating motion considerably enhanced the coil sensitivity encoding capability, making higher reduction factors in scan time possible. The sensitivity encoding capability can be further improved by choosing an optimal speed of array rotation. Compared to traditional phased-array coils (PACs) with twice as many coil elements, the RRFCA demonstrated clear advantages in terms of quality of reconstruction and superior noise behaviour in all the cases investigated in this initial study.**

## I. Introduction

Long acquisition times in magnetic resonance imaging (MRI) can cause physiological motion artefacts and add discomfort to patients. Consequently, minimising scan time without compromising image quality has been one of the main thrusts for MRI research since the establishment of the field. Broadly speaking, two main approaches have been developed for MR imaging acceleration: (1) full k-space scanning using fast pulse sequences [1-3]; (2) k-space sub-sampling using parallel imaging or sparse sampling [4-7].

To reconstruct full field-of-view images from partial k-space acquisition, parallel imaging (PI) has been successfully applied in clinical applications. In PI, multiple receiver radiofrequency (RF) coils are used to implement simultaneous k-space under-sampling. The image is then reconstructed with the help of sensitivity encoding provided by multiple receiver RF coils. There are many different reconstruction algorithms, such as: SENSitivity Encoding (SENSE) [4, 5], Simultaneous Acquisition of Spatial Harmonics (SMASH) [6] and Generalized Autocalibrating Partially Parallel Acquisition (GRAPPA) [7]. SENSE employs multiple receiver RF coils to complement and partially replace gradient encoding, thus reducing k-space data and scan time. In order to obtain higher acceleration factors, the current trend is to increase the number of RF coils/channels, thereby providing more unique sensitivity encoding functions. However, adding more elements increases electromagnetic coil-to-coil coupling interactions and hardware cost.

The rotating RF coil technique has recently been introduced as a novel alternate method, in which a single RF coil (RRFC) is rotated about the patient to induce and receive the MR signals for subsequent image formation [8, 9]. Compared to traditional phased-array coils (PACs), the RRFC has intrinsic advantages, including: no mutual coupling between coil elements and being relatively inexpensive (i.e. only one RF channel and accompanying electronics). In practice, however, the acceleration capability and signal-to-noise performance of the single-element RRFC can be limited by the speed of coil rotation and ill-posed nature of the linear system equation [10, 11].

In the current study, a four-element low-density naturally-decoupled rotating radiofrequency coil array (RRFCA) is modelled and investigated. The proposed coil model has advantages, such as (1) sufficient coil-to-coil separations and, therefore, natural decoupling; (2) low RF channel count implying relatively low hardware cost; and (3) the rotating motion of the array can potentially provide uniform coverage of the imaged subject as well as numerous sensitivity encoding functions. Using electromagnetic models and numerical simulations, the current study investigates the feasibility of such a rotating coil array for accelerated parallel acquisitions. The method of reconstruction and noise behaviour are presented. The performance of the proposed hybrid system is compared with traditional stationary 4- and 8-element arrays at various reduction factors.

## II. Methodology

### *A. Modelling and calculation of $B_1$ fields*

The RRFCA model was an array of RF coils with identical structure evenly distributed around the cylindrical coil former of 300 mm in diameter, which was continuously rotating about the longitudinal axis. In the current study, the RRFCA consisted of a total of 4 elements, each of which was 300 mm in length (longitudinal) and 100 mm in width (transversal). This provided ample distance (130 mm) and sufficient electromagnetic separation between two adjacent elements when loaded (-15 dB). A homogenous spherical head phantom with 125 mm in radius was placed in the isocentre of the gradients system. The RRFCA and phantom geometry are shown in Fig. 1. The permittivity and conductivity of the phantom were 52 and 0.4 S/m respectively, to mimic "average" brain tissue at 128 MHz.

[1]School of Information Technology and Electrical Engineering, University of Queensland, QLD 4072, Australia (e-mail: mingyan@itee.uq.edu.au)

4- and 8-element traditional stationary PACs were also modelled for applications at 128 MHz. The 4-element PACs had the exactly same configuration as the RRFCA, whereas the 8-element PACs adopted 8 coil elements evenly distributed on the coil former. Inductive decoupling circuits were introduced to provide channel isolations of -15 dB. The 4- and 8-channel traditional PACs were loaded with the same homogenous head phantom described previously. The modelling and electromagnetic solutions were performed with the commercially available software package FEKO (EMSS, SA).

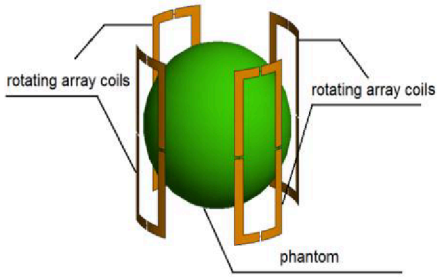

Fig. 1 RRAFC and Phantom Geometry

The circular polarization of steady-state RF magnetic fields ($B_1$) field was calculated as [12]:

$$B_1^+ = (B_x + iB_y) / 2 \quad (1a)$$

$$B_1^- = (B_x - iB_y)^* / 2 \quad (1b)$$

where $B_1^+$, $B_1^-$, $B_x$ and $B_y$ are position dependent complex magnetic field quantities; $B_x$ and $B_y$ are vector components calculated from numerical calculations; $i$ is the imaginary unit; * asterisk indicates the complex conjugation.

### *B. Reconstruction and noise propagation*

In SENSE, the net encoding function does not obey the conventional full Fourier encoding, as coil sensitivity is also used as a means of signal encoding [5]. Consequently, the density of k-space samples can be reduced and replaced by sensitivity encoding, thereby accelerating the image acquisition time. However, as a result, the image reconstruction cannot be performed by 2D inverse Fourier transform. The general method to reconstruct an image is to solve a system matrix:

$$\mathbf{A}x = \mathbf{b} \quad (2)$$

where **A** is the reconstruction matrix; x is the unknown image; **b** is the k-space data acquired in the experiment, arranged in a vector of size $(n_c \times n_k) \times 1$, where $n_c$ and $n_k$ denote the number of receiver coils and the number of sampling positions in k-space, respectively.

The element in matrix A is:

$$E_{(\gamma,k)\rho} = e^{i\mathbf{k}_\kappa r_\rho} \mathbf{S}_\gamma(\boldsymbol{r}_\rho) \quad (3)$$

where $\boldsymbol{r}_\rho$ denotes the position of the ρ-th voxel; $\mathbf{k}_\kappa$ is the κ-th sampling position in k-space; and $\mathbf{S}_\gamma$ is the complex spatial sensitivity of the γ-th coil. The size of A is $(n_c \times n_k) \times N_v$, where $N_v$ is the number of points to be resolved in image domain. In matrix form, **A** is given by:

$$A = \begin{bmatrix} \begin{pmatrix} e^{i\mathbf{k}_1 r_1}\mathbf{S}_1(\boldsymbol{r}_1) & \cdots & e^{i\mathbf{k}_1 r_N}\mathbf{S}_1(\boldsymbol{r}_N) \\ \vdots & \ddots & \vdots \\ e^{i\mathbf{k}_{n_k} r_N}\mathbf{S}_1(\boldsymbol{r}_1) & \cdots & e^{i\mathbf{k}_{n_k} r_N}\mathbf{S}_1(\boldsymbol{r}_N) \end{pmatrix} \\ \vdots \\ \begin{pmatrix} e^{i\mathbf{k}_1 r_1}\mathbf{S}_{n_c}(\boldsymbol{r}_1) & \cdots & e^{i\mathbf{k}_1 r_N}\mathbf{S}_{n_c}(\boldsymbol{r}_N) \\ \vdots & \ddots & \vdots \\ e^{i\mathbf{k}_{n_k} r_N}\mathbf{S}_{n_c}(\boldsymbol{r}_1) & \cdots & e^{i\mathbf{k}_{n_k} r_N}\mathbf{S}_{n_c}(\boldsymbol{r}_N) \end{pmatrix} \end{bmatrix} \quad (4)$$

where A is formed by concatenating $n_c$ blocks of matrices, each of which represents the encoding matrix of the corresponding coil.

For traditional stationary PACs, since the array remains stationary during the course of acquisition, the sensitivity profiles remain unchanged from row to row within the same block. However, the encoding matrix for the RRFCA was modified to account for the changing sensitivity profile from sample to sample due to continuous rotating motion. The encoding matrix for RRFCA $A^R$ reads:

$$A^R = \begin{bmatrix} \begin{pmatrix} e^{i\mathbf{k}_1 r_1}\mathbf{S}_{1(t_1)}(\boldsymbol{r}_1) & \cdots & e^{i\mathbf{k}_1 r_N}\mathbf{S}_{1(t_1)}(\boldsymbol{r}_N) \\ \vdots & \ddots & \vdots \\ e^{i\mathbf{k}_{n_k} r_N}\mathbf{S}_{1(t_N)}(\boldsymbol{r}_1) & \cdots & e^{i\mathbf{k}_{n_k} r_N}\mathbf{S}_{1(t_N)}(\boldsymbol{r}_N) \end{pmatrix} \\ \vdots \\ \begin{pmatrix} e^{i\mathbf{k}_1 r_1}\mathbf{S}_{n_{c(t_1)}}(\boldsymbol{r}_1) & \cdots & e^{i\mathbf{k}_1 r_N}\mathbf{S}_{n_{c(t_1)}}(\boldsymbol{r}_N) \\ \vdots & \ddots & \vdots \\ e^{i\mathbf{k}_{n_k} r_N}\mathbf{S}_{n_{c(t_N)}}(\boldsymbol{r}_1) & \cdots & e^{i\mathbf{k}_{n_k} r_N}\mathbf{S}_{n_{c(t_N)}}(\boldsymbol{r}_N) \end{pmatrix} \end{bmatrix} \quad (5)$$

From Eq. (5), it is clear that the Fourier encoding kernel is consistent between the stationary and rotating array; however each row has different sensitivity values as the coil sensitivity rotates.

### *C. Noise in SENSE Images*

To solve Eq. (2) in parallel imaging, matrix inversion needs to be performed. The general solution has the form $x=A^{-1}b$. If the simultaneous equations to be solved are similar, the solutions are generally sensitive to small changes in b, i.e. noise in the k-space acquisitions. In extreme situations, if the equations are very similar, which could be caused by two coils very close to each other, or due to a small field of view, it is difficult to arrive at an optimal solution, as solutions are likely to be dominated by noise [13].

Parallel imaging reconstructions result in spatially varying noise amplification which is characterized by the g-factor (geometry factor) [14]. The calculation of the g-map is given as [4]:

$$g_\rho = \sqrt{[(S^H \psi^{-1} S)^{-1}]_{\rho,\rho} (S^H \psi^{-1} S)_{\rho,\rho}} \geq 1 \quad (6)$$

where ρ denotes the voxel under consideration within the set of voxels to be separated, and $\psi$ is the receiver noise correlation matrix.

The g-factor indicates, for a particular voxel, the noise levels of reduced sampling as compared with full k-space sampling. A similar analysis for noise propagation in the case of RRFCA was performed. The encoding matrix A was first represented as multiplications of two matrices:

$$A = F \times S \tag{7}$$

where $F$ denotes Fourier encoding matrix; $S$ denotes sensitivity encoding matrix. Eq.(7) delineates Fourier and sensitivity encoding, so that the matrix S can be used with Eq.6 to provide g-map calculation [15].

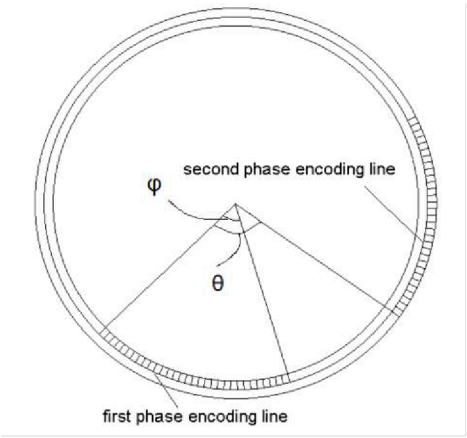


Fig. 2 Assuming 32 × 32 k-space data are sampled counter-clockwisely. In this figure only 2 first k-space line sampling were shown. Each circle and a grid represented a k-space line and a k-space sample point respectively. The start position of first k-space sample was at left of first phase encoding line.

### *D. Optimisation of Sensitivity Encoding*

The quality of the solution to Eq.2 is depended primarily on the condition of encoding matrix $A$ or $A^R$. Comparing Eq.4 to Eq.5, it was clear that the varying sensitivity encoding in RRFCA could potentially enhance the sensitivity encoding ability compared with the stationary coil arrays.

Moreover, the imaging parameters could be strategically chosen to further improve the sensitivity encoding capability of the RRFCA. Employing RRFCA, the first and second phase encoding lines of a Fast Low Angle Shot (FLASH) imaging sequence is shown in Fig. 2. The angular displacement between the beginning positions of two adjacent phase-encoding acquisitions was:

$$\theta = (TR \times \omega) \backslash (2\pi) \tag{8}$$

where operator '\' takes the remainder of the division. The angular span of the RRFCA during one phase-encoding line acquisition was:

$$\emptyset = T_{Acq} \times \omega \tag{9}$$

where $T_{Acq}$ denotes acquisition time of each phase-encoding line. Clearly, $\theta$ and $\emptyset$ had direct impact on g-factor and the condition of the encoding matrix $A^R$. While the time of repetition (TR) was chosen to provide an optimal tissue contrast and $T_{Acq}$ was typically on the order of several milliseconds, $\omega$ could be optimised to yield the best combination of $\theta$ and $\emptyset$ to facilitate the g-factor minimisation and, therefore, the optimisation of sensitivity encoding.

## III. RESULTS

Fig. 3 shows the g-maps of the optimised and the non-optimised 4-element RRFCA and 8- and 4-element PACS. It can be seen that the non-optimised RRFCA, as compared with the stationary 4-element array with the same geometry, presents much improved g-map and maximum g-factor when, R was 2, 3 and 4. In fact, the non-optimised RRFCA had similar performance compared with the stationary array with twice as many elements (third column). The optimised RRFCA (first column) demonstrated further improved sensitivity encoding ability. The maximum g-factor of the optimised RRFCA was constantly smaller than that of the 8-element stationary array.

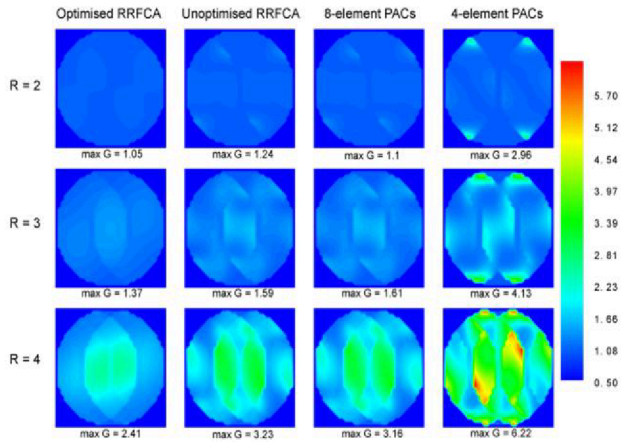


Fig. 3 G-amp comparison when R = 2, 3 and 4 among optimised RRFCA (first column), unoptimised RRFCA (second column), 8-element PACs (third column), 4-element PACs (fourth column). Under all reduction factors, the optimised RRFCA had the lowest max g-factor.

The stationary 8-element PACs and the proposed 4-element RRFCA were used in a simulated parallel imaging study. Fig. 4 shows the original image (a), and reconstructed images for RRFCA (c) and 8-element array coils (d), when R was 4. -40dB Gaussian noise (with respect to signal) was added to the original image in Fig. 4 (b) as described in [16]. Similar reconstruction qualities were achieved by using the optimised 4-element RRFCA (Fig. 4 (c)) and the traditional 8-element stationary array (Fig. 4 (d)). This agreed well with the comparable g- factor between the two coils (i.e., 2.41 versus 3.16).

Error maps were calculated to assist visual comparisons of reconstruction qualities of using two arrays. As compared to reference image in Fig. 4(b), Fig. 5 (a) and (b) demonstrated the reconstruction errors when using 4-element RRFCA and 8-element PACs, respectively. Fold-over artefacts were clearly visible in Fig. 5(b), whereas Fig. 5(a) exhibited improved noise behaviour, in which the artefact were scattered approximately uniformly over the FOV. The root mean square deviation (RMSD) and artefact power (AP) also demonstrated better performance of RRFCA (RMSD: 0.0079 and AP = 3.52e-4) compared to 8-element PACs

(RMSD: 0.0113 and AP = 7.29e-4), respectively. This correlated well with the hypothesis that RRFCA has a better noise-resistance performance than traditional stationary PACs.

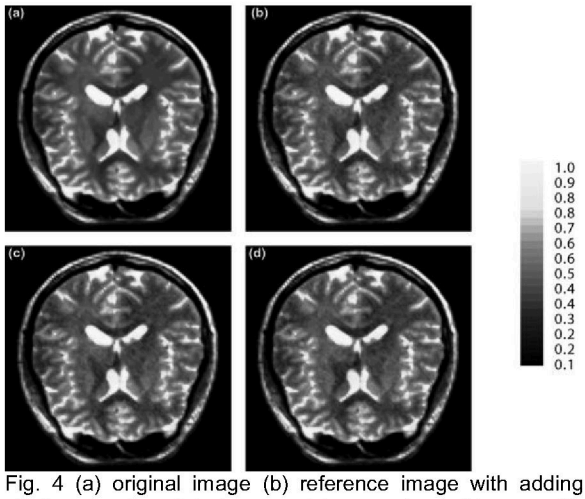


Fig. 4 (a) original image (b) reference image with adding -40db noise to original image (c) reconstructed image with RRFCA (d) reconstructed image with 8-element PACs

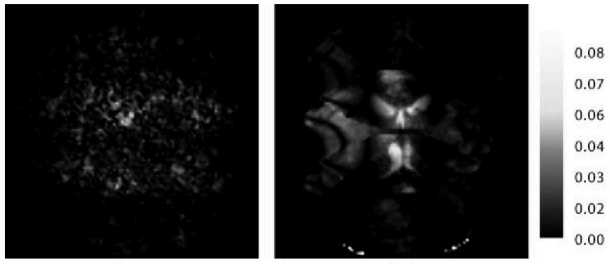


(a) (b)

Fig. 5 Error map (a) RRFCA (b) Traditional PACs

## IV. Conclusion and Discussion

In this proof-of-concept study, a novel hybrid imaging method using a low-density naturally-decoupled rotating RF coil array was investigated. The theory of image reconstruction was studied and the noise propagation was analysed. The calculated g-maps indicated that the proposed coil array was able to provide considerably improved sensitivity encoding compared to traditional stationary array with twice as many elements. In the cases investigated, the 4-element RRFCA achieved a reduction factor of 4 while the maximum g-factor was only around 2.4. Owing to more severe $B_1$ field inhomogeneity, an even lower g-factor can be expected at 7T, especially with heterogeneous subjects. The error maps showed that the rotating sensitivity encoding provided by the RRFCA had an ability to scatter the aliasing artefact in parallel imaging. The RMSD and AP results of RRFCA were significantly better than the transitional 8-element stationary PACs, which presented a quantitative comparison to illustrate the advantages of RRFCA.

The current study provided a theoretical framework of the proposed RRFCA system with preliminary results. Follow-up studies will focus on experimental validations.

## References


[1] P. Mansfield, *et al.*, "Fast scan proton density imaging by NMR," *Journal of Physics E: Scientific Instruments,* vol. 9, p. 271, 1976.

[2] J. Listerud, *et al.*, "First principles of fast spin echo," *Magn Reson Q,* vol. 8, pp. 199-244, Dec 1992.

[3] P. van der Meulen, *et al.*, "Very fast MR imaging by field echoes and small angle excitation," *Magn Reson Imaging,* vol. 3, pp. 297-9, 1985.

[4] K. P. Pruessmann, *et al.*, "SENSE: Sensitivity encoding for fast MRI," *Magnetic Resonance in Medicine,* vol. 42, pp. 952-962, 1999.

[5] K. P. Pruessmann, *et al.*, "Advances in sensitivity encoding with arbitrary k-space trajectories," *Magn Reson Med,* vol. 46, pp. 638-51, Oct 2001.

[6] D. K. Sodickson and W. J. Manning, "Simultaneous acquisition of spatial harmonics (SMASH): Fast imaging with radiofrequency coil arrays," *Magnetic Resonance in Medicine,* vol. 38, pp. 591-603, 1997.

[7] M. A. Griswold, *et al.*, "Generalized autocalibrating partially parallel acquisitions (GRAPPA)," *Magnetic Resonance in Medicine,* vol. 47, pp. 1202-1210, 2002.

[8] A. Trakic, *et al.*, "A rapidly rotating RF coil for MRI," *Concepts in Magnetic Resonance Part B: Magnetic Resonance Engineering,* vol. 35B, pp. 59-66, 2009.

[9] A. Trakic, *et al.*, "Image reconstructions with the rotating RF coil," *Journal of Magnetic Resonance,* vol. 201, pp. 186-198, 2009.

[10] D. C. Alsop, *et al.*, "A spiral volume coil for improved RF field homogeneity at high static magnetic field strength," *Magnetic Resonance in Medicine,* vol. 40, pp. 49-54, 1998.

[11] Y. Li, *et al.*, "A modelling study of a Hybrid Loop-Strip coil structure for multichannel Transceive Breast Array Coil," presented at the ISMRM-ESMRMB joint annual meeting, Stockholm, Sweden, 2010.

[12] D. I. Hoult, "The principle of reciprocity in signal strength calculations—A mathematical guide," *Concepts in Magnetic Resonance,* vol. 12, pp. 173-187, 2000.

[13] D. Larkman, "The g-Factor and Coil Design
Parallel Imaging in Clinical MR Applications," S. O. Schoenberg, *et al.*, Eds., ed: Springer Berlin Heidelberg, 2007, pp. 37-48.

[14] P. M. Robson, *et al.*, "Comprehensive quantification of signal-to-noise ratio and g-factor for image-based and k-space-based parallel imaging reconstructions," *Magn Reson Med,* vol. 60, pp. 895-907, Oct 2008.

[15] E. K. Insko and L. Bolinger, "Mapping of the radiofrequency field," *Journal of Magnetic Resonance, Series A,* vol. 103, pp. 82-85, 1993.

[16] J. Jin, *et al.*, "An electromagnetic reverse method of coil sensitivity mapping for parallel MRI – Theoretical framework," *Journal of Magnetic Resonance,* vol. 207, pp. 59-68, 2010.